Physica Scripta,vol.79, pp1-12, 2009
Print ISSN: 0031-8949
Online ISSN: 1402-4896
doi: 10.1088/0031-8949/79/05/055301

0Thttp://journals.iop.org/
http://www.iop.org/EJ/journal/PhysScr
This is an un-copyedited version of an article accepted for publication in Phys. Scr. IOP Publishing Ltd is not responsible for any errors or omissions in this version of the manuscript or any version derived from it. The definitive publisher authenticated version is available online at doi: 10.1088/0031-8949/79/05/055301

Recombination rate coefficients for KLL dielectronic satellite lines of Fe XXV and Ni XXVII

S N Nahar[1], J Oelgoetz[2,3] and A K Pradhan[1]

[1] Department of Astronomy, The Ohio State University, Columbus, OH 43210, USA
[2] Applied Physics Division, Los Alamos National Laboratory, Box 1336, Mail Stop F663, Los Alamos, NM 87545, USA

E-mail: nahar@astronomy.ohio-state.edu, oelgoetz@lanl.gov and pradhan@astronomy.ohio-state.edu

Abstract
The unified method for total electron-ion recombination is extended to study the dielectronic satellite (DES) lines. These lines, formed from radiative decay of autoionizing states, are highly sensitive temperature diagnostics of astrophysical and laboratory plasma sources. The computation of the unified recombination rates is based on the relativistic Breit-Pauli R-matrix method and the close coupling approximation. As such unified recombination cross sections (σ_{RC}) include both the resonant and the non-resonant background contributions and the DES spectra correspond directly to resonances in σ_{RC}. Extending the theoretical formulation developed earlier (Nahar and Pradhan 2006 *Phys. Rev.* A **73** 062718-1) we present recombination rate coefficients for the 22 satellite lines of KLL complexes of helium-like Fe XXV and Ni XXVII. The isolated resonance approximation, commonly used throughout plasma modeling, treats these resonances essentially as bound features except for dielectronic capture into, and autoionization out of, these levels. A line profile or cross section shape is often assumed. On the other hand, by including the coupling between the autoionizing and continuum channels, the unified method gives the *intrinsic* spectrum of DES lines which includes not only the energies and strengths, but also the natural line or cross section shapes. A formulation is presented to derive autoionization rates from unified resonance strengths and enable correspondence with the isolated resonance approximation. While the rates compare very well with existing rates for the strong lines to <20%, the differences for weaker DES lines are larger. We also illustrate the application of the present results to the analysis of K**a** complexes observed in high-temperature x-ray emission spectra of Fe XXV and Ni XXVII. There are considerable differences with previous results in the total KLL intensity for Fe XXV at temperatures below the temperature of maximum abundance in coronal equilibrium.

1. Introduction

The dielectronic satellite (DES) lines are commonly seen in the spectra of highly ionized ions in high-temperature sources, such as active and flaring regions of the solar corona or fusion devices (Bely-Dubau *et al* 1982, Kato *et al* 1998). They have been shown to be of particular relevance as diagnostics of both steady-state and transient stages of a plasma source (Oelgoetz and Pradhan 2001, 2004). The physical process entails the collision of an electron with an N-electron ion core, forming an $(N + 1)$-electron quasi-bound, doubly excited resonant state, which may decay radiatively or via autoionization (AI). Radiative decay leads to recombination of the free electron

[3] Present address: Department of Physics and Astronomy, Austin Peay State University, P. O. Box 4608, Clarksville, TN37044, USA. Email: oelgoetzj@apsu.edu

into a stabilized bound state of the (N + 1)-electron ion—the process known as dielectronic recombination (DR). For highly charged ions of relatively heavy elements, the large radiative decay rates in the parent ion core compete effectively with the

AI rates for the (e + ion) system. Schematically, this branching process may be written as

$$e + X^{++} \leftrightarrow (X^{+})^{**} \leftrightarrow \begin{cases} e + X^{++}(\mathrm{AI}), \\ h\nu + X^{+}(\mathrm{DR}). \end{cases} \qquad (1)$$

The doubly excited, autoionizing state (denoted by a double asterisk) appears as a resonance that breaks up either via autoionization, a radiation-less transition back to the N-electron ion and a free electron carrying away the excess energy into the continuum, or via radiative stabilization to a recombined $(N+1)$-electron bound state. In the latter case the excited ion core decays radiatively via a strong dipole transition, usually into a low-lying state, and the incident electron is thereby captured into an $(N+1)$-electron state; the resulting photon emission manifests itself as a DES line. The radiative transition within the N-electron ion core is called a *principal* transition. The DES lines are somewhat lower in energy, thus at longer wavelengths or 'redward' of, the principal line. There is an infinite set of these DES lines corresponding to the Rydberg series of autoionizing levels as $n \rightarrow \infty$, converging onto the threshold for the principal core transition. Only the lowest n-complexes are usually observed and resolved however, as they have larger electron-capture rates (inverse of AI rates) and are sufficiently removed energetically from the principal transition. The higher-n DES lines blend with the principal line.

The strongest DES lines stem from the n = 2 complex in He-like ions, and are 'satellites' to the principal transition $1s2p\ ^1P^o_1 \rightarrow 1s^2\ ^1S_0$, designated as the line w (also referred to as the 'resonance transition'). The w-line wavelengths for Fe XXV and Ni XXVII are 1.8504 and 1.5884 Å, respectively. The recombining electron forms a three-electron Li-like system in a quasi-bound state that may decay radiatively. The doubly excited autoionizing states corresponding to the n = 2 complex ($1s2l2l'$) are designated as KLL resonances. Radiative decay of the KLL resonances to Li-like bound states ($1s^22s^2S_{1/2}$, $1s^22p^2P^o_{1/2}$ and $1s^22p^2P^o_{3/2}$) give rise to 22 DES lines. The KLL DES lines from several elements are seen in high-temperature plasma sources above 1 MK (Beieresdorfer *et al* 1992, Kato *et al* 1998). In order for the DES lines to form, the plasma temperature must be sufficiently high such that energetic electrons are available to recombine with the target ion via these quasi-bound states. A DES line arises from electrons in a very narrow energy range corresponding to a particular AI level and its width. But the principal line can be excited by any electron with an energy greater than the threshold energy of excitation of the core transition. In other words, the DES line is sensitive to a single free-electron energy, whereas the excitation of the principal line depends largely on the electron distribution, generally a Maxwellian with a specific temperature. Therefore, the ratio of a DES line to the principal line in the core (the aforementioned w-line in the case of KLL resonances) is very sensitive to the plasma temperature. It follows that DES lines weaken much faster than the

principal line near and beyond the temperature of maximum abundance (assuming coronal equilibrium).

The formation of DESs may also be viewed as a subset of the electron-ion recombination process. As equation (1) implies, by taking detailed balance into account, (e + ion) recombination is the inverse of photoionization. Recombination is usually divided into multiple components: radiative recombination (RR) which refers to non-resonant or background photo-recombination, DR via autoionizing resonances, and, if appropriate to the plasma, the stimulated analogues of these processes. Previous works (e.g. Nahar and Pradhan 1994, 2004) have developed a method that unifies both the RR and DR processes, accounting for quantum mechanical interference between the two processes.

Nahar and Pradhan (2006) further extended the unified method for total electron–ion recombination for DES lines and showed that the profiles and intensities of the unified recombination cross sections (σ_{RC}) directly correspond to, and compare well with, the measured strengths and observed recombination spectra. We refer to the unified (e + ion) recombination cross section as σ_{RC}, which is the detailed balance inverse of photoionization from all bound states of the (e+ion) system and subsumes both the RR and DR processes. The unified (e + ion) recombination method yields a representation of DES spectra that includes the interference between RR and DR in an *ab initio* manner. This is in contrast to existing isolated resonance approximation (IRA) treatments (such as Bely-Dubau *et al* 1982) that do not include this coupling.

In this report we extend and complete the new approach for DES lines described in Nahar and Pradhan (2006), and demonstrate its use with two important practical examples. We also compute the resonance strengths for KLL DES lines of (e+Fe XXV) and (e+Ni XXVII) to higher precision than in the earlier work. They are presented in two different ways: the theoretical recombination resonance strength and the DES line strength for comparison with experimentally measured values. The theoretical resonance strength is computed from the unified recombination cross sections without approximation and exhibits the full spread of the resonance profile with energy. But the experimentally measured value is obtained to one single (peak) energy; therefore, the DES line strength is recomputed at that energy. In general, this uncertainty in the measured values is not too critical to accuracy for DES resonances where the peak is sharply defined. Finally, the rates for all DES lines are tabulated and should be more accurate than previous works for spectral analysis, potentially applicable to the analysis of x-ray observations from a variety of plasma sources.

2. Theory

As mentioned above, the unified recombination approach for the strengths and rates of DES lines is fundamentally different from existing approaches based on the IRA. In the IRA a DES line is formed when a target ion captures a free electron into an autoionizing state, and this autoionizing state undergoes radiative stabilization via decay to bound (e + ion) state to complete the DR process. This emitted photon is treated just as if it were a bound–bound emission line, thus it is calculated using a standard line profile, centered about a single energy. The unified method, on the other hand, yields the entire line profile in an *ab initio* manner by calculating recombination cross sections from photoionization cross sections that account for the coupling between all of the quasi-bound states and the continuum, and the interference effects between the two, as summarized below.

2.1. The unified method for total recombination cross sections

The basic outline of the calculation starts with the bound *N*-electron wave functions for a number of states of the target ion (χ_i(ion)). In the coupled channel R-matrix methodology, these *N*-electron
wave functions are then used to calculate wave functions for the *(N+1)* electron system (Ψ(ion + e; *E, J,* π*)*, which are defined by an energy *E*, angular momenta *J* and parity π*)* by using the close coupling expansion

$$\Psi(\text{ion}+\text{e};\, E, J, \pi) = \hat{A}\left(\sum_i \chi_i(\text{ion})\theta_i + \sum_j c_j \Phi_j(\text{ion}+\text{e})\right), \tag{2}$$

where χ_i is the target wave function in a specific level J_i π_i and θ_i is the wave function for the *(N+1)*th electron in a channel labeled as S_iL_i $(J_i)\pi_i$ $k_i^2\ell_i(J\pi)$ where k_i^2 is its incident kinetic energy. A channel is open or closed depending on positive or negative energy of the electron. The Φ_j's are correlation functions of the *(N+1)*-electron system that are built from the one-electron wave functions of the *N* electron system and account for short-range correlations and orthogonality between continuum and bound orbitals. It should be noted that in this treatment, autoionizing states are not discrete states, but instead are embedded in the continuum and result from the coupling of open and closed channels. As a consequence the terms autoionizing or quasi-bound states appear naturally with the continuum and are treated together in the unified framework; thus we will use them only to refer to the IRA calculations.

As the coupled channel expansion, equation (1), allows for interaction between the autoionizing states and the continuum, it accounts for quantum mechanical interference between them. Resonances are a consequence of this coupling. The unified method thereby includes both recombination processes, via the continuum (RR), and via autoionizing resonances (DR). In addition, it should also be noted that the same expansion, equation (1), is used for both the bound states *(E* < 0), and for the continuum wave functions *(E* > 0).

Photoionization cross section of a bound level B can be obtained as

$$\sigma_{\text{PI}}(B, E) = \sum_{(J,\pi)} \sigma_{\text{PI}}(B \to J, \pi, E), \tag{3}$$

$$\sigma_{\text{PI}}(B \to J, \pi, E) = \frac{1}{g_i}\frac{4\pi^2}{3c}\omega \mathbf{S}(\mathbf{J}, \pi, \mathbf{E}), \tag{4}$$

$$\mathbf{S} = |\langle \Psi_{\text{B}} \| \mathbf{D} \| \Psi_{\text{F}}(J, \pi, E)\rangle|^2, \tag{5}$$

where *gi* is the statistical weight factor of the initial bound state, Ψ_{B} and Ψ_{F}, respectively, are the bound and free electron wave functions calculated using the expansion presented in (2), and **D** is the dipole operator ($\mathbf{D} = \Sigma_i^{N+1} r_i$).

The radiative decay rates of highly charged H- and He-like recombining ions are often comparable to the Auger rates of autoionizing states, typically 10^{12}–10^{14} s^{-1} (e.g. Nahar *et al* 2000) with strong dipole allowed $2p(^2P^o) \rightarrow 1s(^2S)$ and $1s2p(^1P^o) \rightarrow 1s^2(^1S_0)$ transitions. Because of this it is essential to use a radiative damping treatment that will account for the probability of the absorbed photon being re-emitted via the radiative decay of the final (e + ion) state. These calculations include radiative damping by using the resonance fitting procedure outlined in Sakimoto *et al (*1990), Pradhan and Zhang (1997) and Zhang *et al* (1999).

The photo-recombination cross section, σ_{RC}, is related to the photoionization cross section, σ_{PI}, through the principal of detailed balance as

$$\sigma_{\rm RC}(B,\epsilon) = \frac{\alpha^2}{4}\frac{g_i}{g_j}\frac{(\epsilon+I)^2}{\epsilon}\sigma_{\rm PI}(B,\epsilon+I) \qquad (6)$$

in Rydberg units. Here, α is the fine structure constant, ϵ is the photoelectron energy, gj is the statistical weight of the recombined ion and I is the ionization potential $(E = \epsilon + I)$. The recombination cross section, σ_{RC}, is calculated at a sufficiently large number of energies to delineate the non-resonant background and the resonances (which, when taken together, subsume both radiative and dielectronic recombination processes). It should be noted that (6) is valid for both $\sigma_{PI}(B, E)$ and $\sigma_{PI}(B \rightarrow J, \pi, E)$.

We assume that the recombining ion is in the ground state and recombination can take place into the ground or any of the excited recombined (e + ion) states. Thus we can calculate a total unified σ_{RC} by summing over the final recombined states. It should be noted that a single resonance in the total σ_{RC} might appear in multiple level specific σ_{RC}'s. This is because one free wave function (or autoionizing state in the IRA framework) can often recombine into multiple bound states. (The selection rules for this recombination are the same as the dipole operator, namely: $\Delta\pi = \pm 1$, $\Delta J = \pm 1, 0$ except $\Delta J \neq 0$ for $J = 0$.) As these final states have different energies, different DES emission lines are formed from each pathway. There is no interference between lines arising from the multiple recombination pathways, although the lines do blend in the total recombination cross section because the total cross section is simply a sum of the level-specific cross sections. This should not be confused with interference between RR and DR, as well as the interference between different resonances within the same symmetry $(J\pi)$. These two interference effects are included as a consequence of the close coupling expansion employed in the unified method.

2.2. Resonance strengths, rate coefficients and intensities of DES lines

The resonances in unified recombination cross sections (σ_{RC}) are observed in the emission spectra as DES lines. As explained in Nahar and Pradhan (2006), integration or averaging over the resonance profiles provides the (a) recombination resonance strengths which are *intrinsic* quantities independent of external plasma conditions, and (b) DES intensities which depend mainly on the electron temperature. Following the notation of Nahar and Pradhan (2006), the recombination rate through a satellite line, for an electron temperature T, $(\alpha_s(T))$ can be expressed as the product of a temperature-dependent term $(f(T))$ and a term that is intrinsic to the satellite line ($S_{RC}(s)$). Nahar and Pradhan (2006) define these as

$$\alpha_s(T) = f(T) S_{\mathrm{RC}}(s), \qquad (7)$$

$$f(T) = \frac{4}{\sqrt{2\pi m_e}} \frac{e^{-\epsilon_s/kT}}{(kT)^{3/2}}, \qquad (8)$$

$$S_{\mathrm{RC}}(s) = \int_{E_i}^{E_f} \epsilon \sigma_{\mathrm{RC}}(\epsilon)\, d\epsilon, \qquad (9)$$

where E_i and E_f are the upper and lower bounds for the line *s*, m_e is the mass of the electron, *k* is the Boltzmann constant and ϵ_s is the resonance's peak energy. The temperature-independent part, S_{RC}, is referred to as the *recombination resonance strength.*

As the lines are narrow, and the resonance profiles are fairly symmetric, the computed DES resonance strengths can be compared directly with those derived from measurements of the *satellite line strength (S(s))*, which is related to the recombination resonance strength (S_{RC}(*s*)) approximately as

$$S(s) \approx S_{\mathrm{RC}}(s)/\epsilon_s. \qquad (10)$$

A more convenient expression relating the basic quantities above is

$$\alpha_s(T) = S(s)\epsilon_s f(T) = 0.015484 \frac{\epsilon_s e^{-(\epsilon_s/kT)}}{T^{3/2}} S(s) \qquad (11)$$

which is valid for any satellite line with a narrow energy width. The units employed are: ϵ in Rydbergs (Ry) and σ_{RC} in Megabarns (Mb). The DES strength $S_{RC}(s)$ can be expressed in CGS units via the following conversion: Ry^2 Mb = 4.75109 x 10^{-40} $ergs^2$ cm^2.

One disadvantage inherent in the recombination cross section σ_{RC} is that it may not be used over the entire energy range since it diverges at zero photoelectron energy. Therefore, we also compute the recombination collision strength Ω_{RC} which shows no such divergence since

$$\sigma_{\mathrm{RC}}(\mathrm{Mb}) = \frac{\pi}{g_i k_i^2} \Omega_{\mathrm{RC}} (a_0^2/10^{-18}), \qquad (12)$$

where k_i^2 is the energy of the incident electron (equivalent to the photoelectron energy ϵ). When calculating DES rate coefficients, $\alpha_s(T)$, we employ both the σ_{RC} and Ω_{RC} as a numerical consistency check.

Intensities of the individual DES lines can be obtained as

$$I_s(i \to j, T) = \alpha_s(T) n_i n_e, \qquad (13)$$

where n_i is the density of the target ion and n_e is the electron density. However, it is common, and often more useful when comparing to experiment, to compare the intensity ratio of the

satellite line to the dipole core excitation line. In the case of KLL lines, this is the *w*-line due to the transition $1s2p\ ^1P^o_1 \rightarrow 1s^2\ ^1S_0$. The intensity ratio of a KLL satellite line to the w-line is obtained as

$$\frac{I_s}{I_w} = \frac{\alpha_s}{q_w}, \qquad (14)$$

where q_w is the rate coefficient for collisional excitation from the ground state, into the 1s2p ($^1P^o_1$) state which gives rise to the *w* line. Most of the modeling codes are based on the IRA. They calculate dielectronic capture and recombination rates from AI rates A_a and radiative rates A_r. Hence, it is desirable to establish a correspondence between the present and the earlier approaches by formulating the AI rates (A_a) from unified resonance strengths. This will facilitate the use of the present data in modeling codes that are based on the IRA framework.

DR, in the IRA is a multi-step process, the first step of which is to calculate a dielectronic capture rate (*D*) which is related to the AI rate by

$$D_{m\rightarrow i} = \frac{g_i}{g_m}\frac{h^3 e^{-(\epsilon_s/kT)}}{2(2\pi m_e kT)^{3/2}} A_a(i \rightarrow m), \qquad (15)$$

where *m* is the state of the target ion and *i* refers to the autoionizing state. It should be noted that this result assumes that dielectronic capture is the detailed balance inverse of AI, but does not assume a specific line (resonance) shape, other than that the shape is centered about ϵ_s. The total DR rate coefficient for the satellite line is then simply the product of the dielectronic capture rate and the branching ratio,

$$\alpha_s^{DR}(T) = D_{m\rightarrow i}\frac{A_r(i \rightarrow j)}{\sum_l A_r(i \rightarrow l) + \sum_k A_a(i \rightarrow k)}, \qquad (16)$$

where an ion in state *m* captures an electron to form autoionizing state *i*, which then completes the DR process by radiatively stabilizing (decaying) to state *j*. The A_r*'s* are radiative decay rates for this last step. The present approach equates this two-step process to a resonance in the level-specific recombination cross section (σ_{RC}). The resonances in σ_{RC} correspond to complete DES line profiles. Substituting (15) into (16) and approximating α_s^{DR} (T) by $\alpha_s(T)$, one gets

$$4S_{RC} = \frac{g_i}{g_m}\frac{h^3}{4\pi m_e} A_a(i \rightarrow n)\frac{A_r(i \rightarrow j)}{\sum_l A_r(i \rightarrow l) + \sum_k A_a(i \rightarrow k)} \qquad (17)$$

which gives the AI rate $A_a(i \rightarrow m)$,

$$A_a(i \rightarrow m) = \frac{S_{RC}}{(g_i/g_m)(h^3/16\pi m_e)A_r(i \rightarrow j) - S_{RC}} \times \left(\sum_l A_r(i \rightarrow l) + \sum_{k\neq m} A_a(i \rightarrow k)\right). \qquad (18)$$

The above equation shows that a given AI rate depends on the degeneracy factors, some constants, $S_{RC}(s)$, the radiative decay rates out of the state, and the other AI rates. Hence if the radiative decay rates are available from another source, A_a for other continuum states can be

obtained by solving the set of coupled linear equations arising from (18) provided the S_{RC} value for the resonances are known. In the case of KLL lines however: $\Sigma_{k\neq m} A_a(i \rightarrow k) = 0$ and the expression simplifies to

$$A_a(i \rightarrow m) = \frac{S_{RC}}{(g_i/g_m)(h^3/16\pi m_e)A_r(i \rightarrow j) - S_{RC}} \sum_l A_r(i \rightarrow l). \quad (19)$$

It should also be noted that this approximation assumes that the RR background in the unified recombination cross section (σ_{RC}) has a negligible contribution to the value of $S_{RC}(s)$ for each and every *s.* In general, this is a reasonable approximation for the systems under consideration in this work.

2.4. Identification and resonance strengths of DES lines

Proper and complete spectroscopic identification of the DES lines with respect to the energy positions is not straightforward from the unified recombination cross sections. The Breit-Pauli R-matrix (BPRM) calculations do not identify resonances spectroscopically *a priori,* as they are formed through coupling or interference of open and closed channels. They can be identified easily from the energy positions of the resonances which are known for ions, such as Fe XXV, from existing experimental values. They can also be determined theoretically from relevant spectroscopic transitions in atomic structure calculations. In our approach, we sort out the DES lines from the level-specific recombination cross sections $\sigma_{RC}(nSLJ)$ by matching the resonances in the cross sections with both the resonances in the total cross section (see Nahar and Pradhan 2006) and the values given in Gabriel (1972).

Again it should be noted that a single resonance in the total recombination cross section may be the sum of individual resonances that appear at the same energy in multiple level-specific cross sections. This is because the same free wave function (or autoionizing state in the IRA framework) can recombine into multiple final states. These resonances, while they do not quantum mechanically interfere, blend together in the total cross section. In such cases $S_{RC}(s)$ must be calculated from the level-specific cross sections.

The fractional contribution of the DES line to the resonance in the total cross section can be determined by examining the contributions of all the constituent lines. The fractions x_s are determined from the ratio of the line strengths, $S_{RC}(s)$, calculated from the level-specific recombination cross sections to the summed strengths $\Sigma_j S_{RC}(j)$, that is, $x_s = S_{RC}(s)/\Sigma_j S_{RC}(s)$.

3. Computation

Computation for the present approach involved extension of existing codes and developing a new code to compute satellite resonance strengths using unified recombination cross sections. The recombination rates of all satellite lines were obtained in four separate computations; the

purpose of the redundancy is to test for numerical problems and consistencies.

Calculations for photoionization and electron–ion recombination are done in several stages, starting with atomic structure calculations using the code SUPERSTRUCTURE (Eissner *et al* 1974) for the target ion wave function. The one-electron orbitals of the target are the initial input to the BPRM suites of codes (Berrington *et al* (1987, 1995), which were developed under the Iron Project (IP), see: Hummer *et al* 1993). The total wave function expansion for the resonance states of Li-like Fe XXIV consists of a 13-level expansion of the target He-like ion, Fe XXV (Nahar *et al* 2001) and a 17-level expansion for Ni XXVII (Nahar 2005). Radiation damping of the resonances is included as described in Zhang *et al* (1999). The present computations for σ_{PI} are confined only to photoelectron energy regions of the first resonance complex, which is the KLL complex, and only to partial photoionization cross sections for leaving the core ion in the ground $1s^2$ (^{1}S0) level.

The level-specific recombination cross sections ($\sigma_{RC}(i)$), collision strengths ($\Omega_{RC}(E, i)$) and rates ($\alpha_R(E, i)$) are computed for all coupled symmetries and levels, and summed to obtain the total using the program PBPRRC (Nahar *et al* 2000). The computation for $\sigma_{RC}(i)$ has been carried out in specified energy ranges (ϵ_i - ϵ_f) corresponding to each satellite line *s* using the extended program RECXS. The total recombination rate coefficients, α_R, are also obtained from the total recombination collision strength, Ω_{RC}. The difference between the two numerical values is a few percent.

A new code SATLN is written to process unified $\sigma_{RC}(i)$ and obtain various quantities, such as the location and identification of the satellite lines, the DES strengths, $S_{RC}(s)$ and $S(s)$, and the recombination rate coefficients of the individual and integrated satellite strengths, as well as to carry out internal consistency checks. The program also determines the individual satellite line contributions to blended resonances in the recombination spectra.

We perform several checks on the numerical accuracy of the calculations, as well as to ascertain if background contributions to DES intensities are negligible. The recombination rate coefficients were obtained in four different ways. The first set of rates was obtained by summing the contributions of level-specific recombination rate coefficients for each of the final three $J\pi$ symmetries responsible for the DES spectra. The second set of rates was obtained from integration of the total recombination collision strengths calculated directly from photoionization cross sections, and including background cross sections for recombination into high-*n* states (comprising the RR contribution). The third set of results is obtained via integration of total σ_{RC} for the entire energy range of the KLL complex, multiplied by the Maxwellian temperature factor $f(t)$ (see (8)). The fourth set of calculations is to compute the DES rates individually. The rate coefficients from all four separate calculations are in good agreement with each other, providing a numerical consistency check as well as validation that the background contributions due to RR are not significant.

4. Results and discussions

Results for Fe XXV and Ni XXVII from the new approach using a unified method for positions, strengths, recombination rate coefficients and intensities of the DES lines are discussed in the subsections below.

4.1. Recombination spectrum of DES lines: profiles and energies

The unified method for total electron–ion recombination can generate the recombination spectrum of DES lines including the background as shown in figure 1 for Fe XXV and figure 2

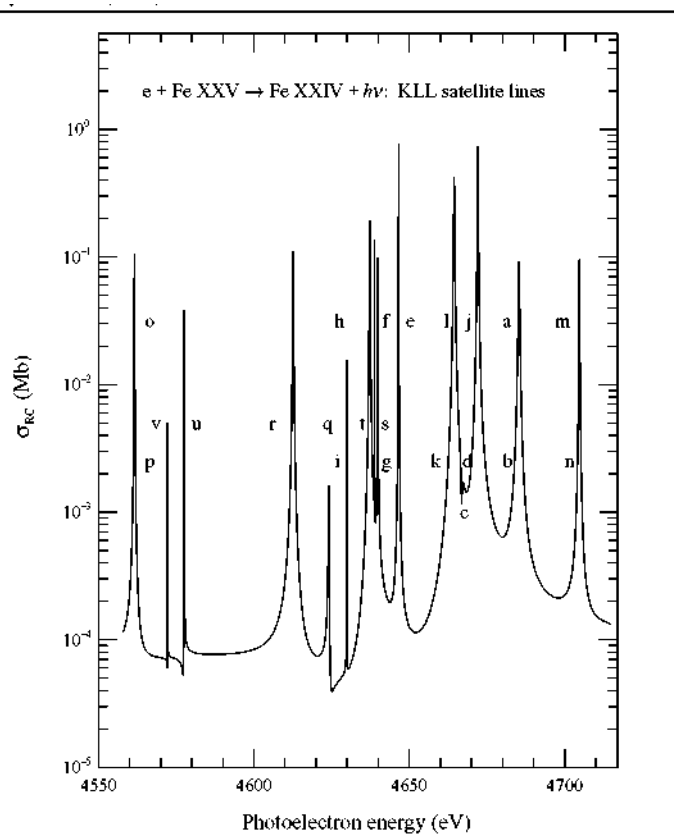

Figure 1. Theoretical profiles of the 22 DES lines of the *Kα* complex seen in unified recombination cross sections of Fe XXV. The interference effects in the *ab initio* results manifest themselves in the natural overlap of line profiles as described in the text.

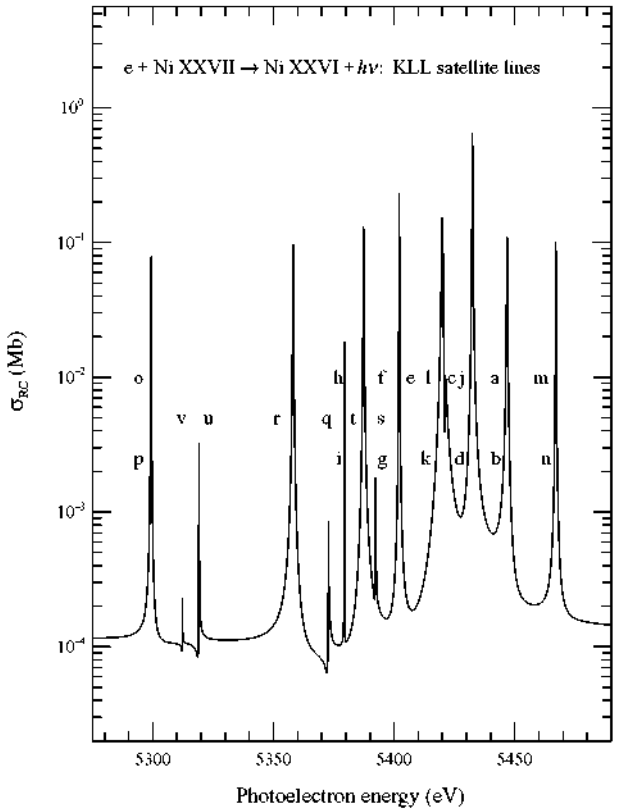

Figure 2. Theoretical profiles of the 22 DES lines of the Kα complex seen in unified recombination cross sections of Ni XXVII, as in figure 1.

for Ni XXVII. The autoionizing resonances in the KLL complex of a He-like ion that appear in the total unified σ_{RC} are the DES lines and provide the relevant physical quantities of the satellite lines. As mentioned previously, the resonances are formed via a process that is analogous to the radiative decay of the autoionizing states arising from the set of configurations 1s2*l*2*l*' into the three $n = 2$ levels: $1s^2 2s^2 S_{1/2}$, $1s^2 2p^2 P^o_{1/2}$, and $1s^2 2p^2 P^o_{3/2}$. The 22 KLL resonances or satellite lines for the two ions are listed in tables 1 and 2.

The interference effects of resonant lines, not considered in IRA methods, manifest themselves in overlapping satellite profiles (the most prominent example is the interaction of d and k, or c and l). Also included in the total unified recombination cross sections (shown in figures 1 and 2) are the multitude of non-interfering, yet blending lines (o and p, d and c, l and k, etc.). The resolved total recombination spectra show 15 DES lines of Fe XXV and 14 DES lines of Ni XXVII. The satellite resonances vary over orders of magnitude in cross section, with often overlapping profiles *within each symmetry;* these overlapping profiles give rise to interference. The pairs (k + d) and (l + c) in the Fe XXV spectrum not only have overlapping profiles, but one of the resonances in each of the pairs is extremely weak (<1%) and lies in the wings of the other one. We emphasize that the overlap and the resulting uncertainty are natural features, which are commonly neglected by IRA methods.

Owing to the natural widths of autoionizing resonances, satellite line profiles in the unified spectrum overlap. These overlaps can be significant in determining satellite intensities, particularly those of the weaker satellites. This also implies that the satellite lines may be

blended and need to be identified carefully. This is in contrast to IRA methods, based on atomic structure calculations, where level designations are initially pre-specified according to the configuration, term, and level structure. As explained above, the lines are identified from the individual $J\pi$ contributions to the level-specific recombination cross sections that contain the resonances. Thus the KLL lines are identified from the individual $J\pi$ contributions to the recombination cross sections into the three Li-like levels $1s^22s^2S_{1/2}$, $1s^22p^2P^o_{1/2}$ and $1s^22p^2P^o_{3/2}$. All 22 satellites in the $n = 2$ Kα complex have been isolated and identified for both Fe XXV and Ni XXVII. The DES are labeled following the notation by Gabriel (1972).

The energies of the satellite lines are assumed to be the peaks of the line profiles and are given in tables 1 and 2 for Fe XXV and Ni XXVII, respectively. The present theoretical energies for Fe XXV agree well with previous calculations. Comparison with EBIT measurements (Beiersdorfer *et al* 1992) shows that the experimental energies are systematically lower than theoretical energies by up to 8eV (~0.1%). This may be taken as the uncertainty in the present calculations. Comparisons of energies and resonance strengths are presented in Nahar and Pradhan (2006). We do not know of experimental data on the Ni XXVII DES lines.

4.2. Strengths and recombination rates of DES lines

The unified recombination cross sections (σ_{RC}) provide the absolute resonance strengths, $S(s)$ and $S_{RC}(s)$, of the DES

Table 1. The 22 DES lines of KLL complex in recombination of (e+Fe XXV): the alphabetic notation (following Gabriel 1972), corresponding resonant transition, experimentally measured energy position E_{ex}, computed energy position in the unified method E_P, satellite strengths S(s) in 10^{-20} cm^2 eV, recombination resonance strength S_{RC} in 10^{-40} cm^2 erg^2 and fractional contribution x_s to each resolved DES lines.

Index		Transition	E_{ex} eV	E_P eV	S(s)	S_{RC}	x_s
1	o	$1s2s^2(^2S_{1/2}) \rightarrow 1s^22p(^2P^o_{3/2})$	4553.4	4561.53	0.8832	1.034	0.50
2	p	$1s2s^2(^2S_{1/2}) \rightarrow 1s^22p(^2P^o_{1/2})$	4553.4	4561.54	0.8820	1.033	0.50
3	v	$1s2p^3P^o\,2s(^4P^o_{1/2}) \rightarrow 1s^22s(^2S_{1/2})$	4573.9	4572.19	0.05994	0.07033	1.00
4	u	$1s2p^3P^o\,2s(^4P^o_{3/2}) \rightarrow 1s^22s(^2S_{1/2})$	4578.9	4577.52	0.1628	0.1913	1.00
5	r	$1s2p^1P^o\,2s(^2P^o_{1/2}) \rightarrow 1s^22s(^2S_{1/2})$	4615.1	4612.63	3.798	4.495	1.00
6	q	$1s2p^1P^o\,2s(^2P^o_{3/2}) \rightarrow 1s^22s(^2S_{1/2})$	4625.3	4622.54	0.08194	0.09721	1.00
7	i	$1s2p^2(^4P_{1/2}) \rightarrow 1s^22p(^2P^o_{1/2})$	4624.6	4629.91	0.07853	0.09331	0.93
8	h	$1s2p^2(^4P_{1/2}) \rightarrow 1s^22p(^2P^o_{3/2})$	4624.6	4629.92	0.00554	0.00659	0.07
9	t	$1s2p^3P^o\,2s(^2P^o_{1/2}) \rightarrow 1s^22s(^2S_{1/2})$	4632.9	4635.60	5.517	6.564	1.00
10	g	$1s2p^2(^4P_{3/2}) \rightarrow 1s^22p(^2P^o_{1/2})$	4639.4	4638.77	0.01199	0.01427	0.03
11	f	$1s2p^2(^4P_{3/2}) \rightarrow 1s^22p(^2P^o_{3/2})$	4632.9	4638.77	0.3721	0.4430	0.97
12	s	$1s2p^3P^o\,2s(^2P^o_{3/2}) \rightarrow 1s^22s(^2S_{1/2})$	4642.5	4639.79	1.291	1.538	1.00
13	e	$1s2p^2(^4P_{5/2}) \rightarrow 1s^22p(^2P^o_{3/2})$	4639.0	4646.57	0.4849	5.783	1.00
14	k	$1s2p^2(^2D_{3/2}) \rightarrow 1s^22p(^2P^o_{1/2})$	4658.1	4664.43	17.43	20.85	0.92
15	l	$1s2p^2(^2D_{3/2}) \rightarrow 1s^22p(^2P^o_{3/2})$	4658.1	4664.43	1.445	1.729	0.08
16	d	$1s2p^2(^2P_{1/2}) \rightarrow 1s^22p(^2P^o_{1/2})$	4658.6	4667.21	0.7809	0.9354	0.82
17	c	$1s2p^2(^2P_{1/2}) \rightarrow 1s^22p(^2P^o_{3/2})$	4658.6	4666.78	0.1703	0.2040	0.18
18	j	$1s2p^2(^2D_{5/2}) \rightarrow 1s^22p(^2P^o_{3/2})$	4664.1	4672.05	26.82	32.18	1.00
19	a	$1s2p^2(^2P_{3/2}) \rightarrow 1s^22p(^2P^o_{3/2})$	4677.0	4685.28	6.118	7.359	0.97
20	b	$1s2p^2(^2P_{3/2}) \rightarrow 1s^22p(^2P^o_{1/2})$	4677.0	4685.30	0.2116	0.2546	0.03
21	m	$1s2p^2(^2S_{1/2}) \rightarrow 1s^22p(^2P^o_{3/2})$	4697.7	4705.47	2.753	3.326	0.95
22	n	$1s2p^2(^2S_{1/2}) \rightarrow 1s^22p(^2P^o_{1/2})$	4697.7	4704.73	0.1301	0.1571	0.05

Table 2. The 22 DES lines of KLL complex in recombination of (e+Ni XXVI): the alphabetic notation (following Gabriel 1972), corresponding resonant transition, computed energy in the unified method E_P, satellite strengths S(s) in 10^{-20} cm^2 eV, recombination resonance strength S_{RC} in 10^{-40} cm^2 erg^2 and fractional contribution x_s to each resolved DES lines.

Index		Transition	E_P eV	S(s) eV	S_{RC}	x_s
1	o	$1s2s^2(^2S_{1/2}) \rightarrow 1s^22p(^2P^o_{3/2})$	5299.32	0.9864	1.341	0.47
2	p	$1s2s^2(^2S_{1/2}) \rightarrow 1s^22p(^2P^o_{1/2})$	5299.32	1.115	1.516	0.53
3	v	$1s2p^3P^o2s(^4P^o_{1/2}) \rightarrow 1s^22s(^2S_{1/2})$	5312.25	0.07304	0.09958	1.00
4	u	$1s2p^3P^o2s(^4P^o_{3/2}) \rightarrow 1s^22s(^2S_{1/2})$	5319.17	0.1765	0.2410	1.00
5	r	$1s2p^1P^o2s(^2P^o_{1/2}) \rightarrow 1s^22s(^2S_{1/2})$	5358.17	4.256	5.852	1.00
6	q	$1s2p^1P^o2s(^2P^o_{3/2}) \rightarrow 1s^22s(^2S_{1/2})$	5372.30	0.1059	0.1461	1.00
7	i	$1s2p^2(^4P_{1/2}) \rightarrow 1s^22p(^2P^o_{1/2})$	5379.37	0.2769	0.3823	0.98
8	h	$1s2p^2(^4P_{1/2}) \rightarrow 1s^22p(^2P^o_{3/2})$	5379.37	0.00427	0.005885	0.02
9	t	$1s2p^3P^o2s(^2P^o_{1/2}) \rightarrow 1s^22s(^2S_{1/2})$	5387.31	5.364	7.415	1.00
10	s	$1s2p^3P^o2s(^2P^o_{3/2}) \rightarrow 1s^22s(^2S_{1/2})$	5392.30	0.1284	0.1777	0.81
11	g	$1s2p^2(^4P_{3/2}) \rightarrow 1s^22p(^2P^o_{1/2})$	5392.41	0.00379	0.005241	0.02
12	f	$1s2p^2(^4P_{3/2}) \rightarrow 1s^22p(^2P^o_{3/2})$	5392.41	0.02548	0.03.527	0.16
13	e	$1s2p^2(^4P_{5/2}) \rightarrow 1s^22p(^2P^o_{3/2})$	5402.16	5.401	7.489	1.00
14	k	$1s2p^2(^2D_{3/2}) \rightarrow 1s^22p(^2P^o_{1/2})$	5419.96	6.380	8.866	0.51
15	l	$1s2p^2(^2D_{3/2}) \rightarrow 1s^22p(^2P^o_{3/2})$	5419.96	6.100	8.477	0.49
16	d	$1s2p^2(^2P_{1/2}) \rightarrow 1s^22p(^2P^o_{1/2})$	5421.21	1.161	1.617	0.50
17	c	$1s2p^2(^2P_{1/2}) \rightarrow 1s^22p(^2P^o_{3/2})$	5421.21	1.151	1.602	0.50
18	j	$1s2p^2(^2D_{5/2}) \rightarrow 1s^22p(^2P^o_{3/2})$	5432.44	25.04	34.92	1.00
19	a	$1s2p^2(^2P_{3/2}) \rightarrow 1s^22p(^2P^o_{3/2})$	5446.84	5.993	8.380	0.96
20	b	$1s2p^2(^2P_{3/2}) \rightarrow 1s^22p(^2P^o_{1/2})$	5446.84	0.2348	0.3283	0.04
21	m	$1s2p^2(^2S_{1/2}) \rightarrow 1s^22p(^2P^o_{3/2})$	5467.02	2.328	3.267	0.78
22	n	$1s2p^2(^2S_{1/2}) \rightarrow 1s^22p(^2P^o_{1/2})$	5467.02	0.6634	0.9.310	0.22

lines by direct integration. Evaluation of individual resonance strengths may have some uncertainties due to the natural overlap of resonances. However, overlap is not expected to be significant since the dominant contribution to integrated value arises from a narrow energy range around the peak energy.

The integrated resonance strengths $S(s)$ and $S_{RC}(s)$ for each of the DES lines are given in tables 1 and 2 for Fe XXV and Ni XXVII, respectively. Only the strong lines in the total spectra in figures 1 and 2 provide significant rates. We have arranged the DES by order of increasing energy, in hopes that it might be more convenient in comparing with observations or experiments than the commonly used alphabetical order, especially where blends of DES are concerned.

Following satellite identifications, we obtain the fractional contribution, x_s, for each resolved line to the blended recombination feature (e.g. o and p). The x_s values are given in tables 1 and 2. For a few weaker satellites, the interference and overlapping of resonances poses significant uncertainty, such as, for the weak resonances of the pairs (k + d) and (l + c) in the Fe XXV spectrum.

The recombination rate coefficients $(\alpha_s(T))$ for the DES lines are given for the recombined ion Fe XXIV in table 3 and for Ni XXVII in table 4. These are obtained from direct integration of the total unified recombination collision strengths Ω_{RC} as described in the theory section. These rate coefficients are more accurate than those using the approximate formula given in Nahar and Pradhan (2006), since the full energy variation of the exponential function e^{CS} $/kT$ is considered in equation (9), rather the peak value of the resonance. These rates were checked with those obtained from the sum of individual contributions of the level-specific rates for numerical accuracy. The fractions x_s are used for $\alpha_s(T)$ of blended lines.

The DES rate coefficients have been tabulated over a wide temperature range to enable interpolation of α_s at practically any temperature. However, as described above, α_s can also be obtained for any temperature of interest using the recombination strength $S_{RC}(s)$ or $S(s)$ and the temperature factor, $f(T)$. Although the approximation of assuming relatively narrow satellite lines is made in (7)-(9), use of (7)-(9) or (11) is simpler and potentially more accurate.

4.3. Comparison of DES line intensities

Given the high-temperature sensitivity of individual DES lines, it is natural to attempt observations that could provide good temperature diagnostics. The intensity ratios of KLL lines with the *w*-line are computed and presented in figure 3. We calculated q_w from the electron impact excitation collision strengths for the *w*-line computed by Pradhan (1985). There is an excellent agreement with the q_w values from previous calculations by Bely-Dubau *et al* (1982); for example, 3.22×10^{-15} and 3.10×10^{-15} cm^{-3} s^{-1}, respectively, at 10^7 K, and 1.23×10^{-13} and 1.24×10^{-13} cm^{-3} s^{-1} at 2×10^7 K. In more recent R-matrix calculations, Whiteford *et al* (2001) also report very good agreement with Pradhan (1985); though their electronically available data lack the finer temperature resolution of Pradhan (1985). Whiteford *et al* (2001)'s graphical comparisons show negligible differences for dipole allowed transitions (within computational uncertainties, usually estimated at <10% for strong dipole transitions). We have therefore used the better resolved (in temperature) calculations of Pradhan (1985) for the *w*-line. (We note, however, that there may be significant differences for other collisional excitation rates of Fe XXV).

Except for a few astrophysical observations of the solar corona and laboratory experiments such as EBITs, the resolution of individual satellite intensities is rare. On the other hand it is easier, and not uncommon, to observe the

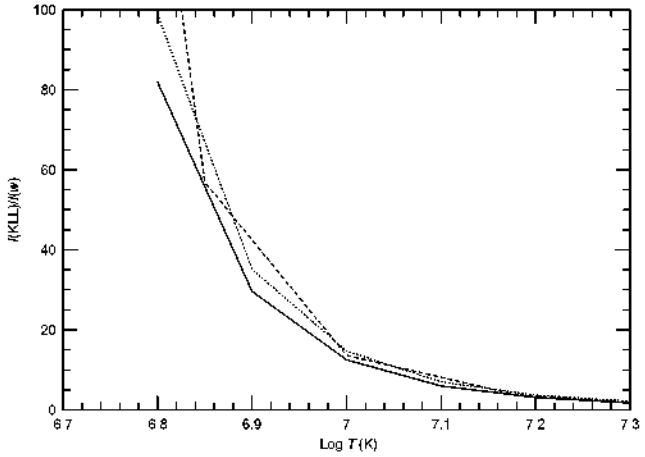

Figure 3. Comparison of intensity ratios I(KLL)/I(w) of Fe XXV with previous calculations: solid line—present, dashed line—Bely-Dubau *et al* (1982), dotted line—Vainshtein and Safronova (1978).

combined intensity of the total KLL DES complex (redward of the *w*-line at one extreme). We therefore compute the intensity ratio I(KLL)/I(w) as a function of temperature.

We compare present intensity ratios of Fe XXV (solid curves) in figure 3 with previous results by Vainshtein and Safronova (1978) (dashed curve) and Bely-Dubau *et al* (1982) (dotted curve), respectively. Figure 3 shows considerable differences in the most sensitive low-temperature range, $T < 2 \times 10^7$ K ($\log(T) = 7.3$); all three sets of results appear to converge to

good agreement as they approach the temperature of maximum abundance of Fe XXV at log(T) ~ 7.4 in coronal equilibrium. But the present values, as well as those of Bely-Dubau *et al* (1982), differ considerably from Vainshtein and Safronova (1978) all throughout by 20% to a factor of two or more. Above log(T) ~ 7.2 our values are in very good agreement with Bely-Dubau *et al* (1982), but show significant differences in the most sensitive region at about log(T) ~ 7.1. In part, the differences as well as the agreement are due to the behavior of the rate coefficient for the resonance w-line which increases with T, while the DES rate is independent of T. Therefore, the satellite-to-resonance line ratio at low temperatures is more reflective of the actual differences between the various approximations employed to compute the DES resonance strengths.

4.4. DES spectra in plasma models

Recently, we have modeled the 6.7 keV complex of Fe XXV and the 7.8 keV complex of Ni XXVII in stationary and transient plasma sources using the new General Spectral Modeling (GSM) code (Oelgoetz 2006, see also: Oelgoetz *et al* 2007a, 2007b). GSM is an IRA code that contains the capability outlined in (19) such that it can calculate AI rates (A_a) from the unified recombination rates of DES lines. The DES spectra for both ions are generated at $T = 10^7$ K and are presented in figures 4 and 5.

To benchmark the present approach, we compare the calculated Fe XXV and Ni XXVII DES spectra using the present unified satellite rates with spectra generated using

Table 3. Recombination rate coefficients for DES lines of Fe XXV forming Fe XXIV (notation: $x–y \rightarrow x$ x10^{-y}).

T(K)	α_R(cm^3 s^{-1})										
	o	p	v	u	r	q	i	h	t	g	f
6.0	3.46–35	3.46–35	2.09–36	5.30–36	8.33–35	1.59–36	1.41–36	9.96–38	9.12–35	1.94–37	6.03–36
6.1	1.31–30	1.31–30	8.10–32	2.09–31	3.56–30	6.99–32	6.29–32	4.44–33	4.14–30	8.85–33	2.75–31
6.2	5.28–27	5.28–27	3.33–28	8.68–28	1.58–26	3.17–28	2.89–28	2.04–29	1.93–26	4.13–29	1.28–27
6.3	3.60–24	3.60–24	2.30–25	6.06–25	1.16–23	2.37–25	2.18–25	1.54–26	1.47–23	3.16–26	9.81–25
6.4	5.97–22	5.96–22	3.87–23	1.02–22	2.05–21	4.22–23	3.92–23	2.77–24	2.67–21	5.75–24	1.79–22
6.5	3.22–20	3.22–20	2.11–21	5.62–21	1.16–19	2.42–21	2.26–21	1.59–22	1.55–19	3.34–22	1.04–20
6.6	7.14–19	7.12–19	4.70–20	1.26–19	2.67–18	5.61–20	5.26–20	3.72–21	3.63–18	7.84–21	2.43–19
6.7	7.78–18	7.77–18	5.16–19	1.39–18	3.01–17	6.35–19	5.98–19	4.22–20	4.15–17	8.96–20	2.78–18
6.8	4.84–17	4.83–17	3.22–18	8.68–18	1.91–16	4.06–18	3.84–18	2.71–19	2.67–16	5.77–19	1.79–17
6.9	1.92–16	1.92–16	1.29–17	3.47–17	7.76–16	1.65–17	1.57–17	1.11–18	1.09–15	2.36–18	7.34–17
7.0	5.36–16	5.35–16	3.59–17	9.73–17	2.20–15	4.69–17	4.46–17	3.15–18	3.12–15	6.74–18	2.09–16
7.1	1.13–15	1.13–15	7.57–17	2.05–16	4.68–15	1.00–16	9.53–17	6.73–18	6.67–15	1.44–17	4.48–16
7.2	1.89–15	1.89–15	1.28–16	3.46–16	7.93–15	1.70–16	1.62–16	1.15–17	1.14–14	2.46–17	7.65–16
7.3	2.67–15	2.66–15	1.80–16	4.89–16	1.13–14	2.42–16	2.31–16	1.63–17	1.62–14	3.51–17	1.09–15
7.4	3.26–15	3.25–15	2.20–16	5.98–16	1.38–14	2.98–16	2.84–16	2.01–17	2.00–14	4.33–17	1.34–15
7.5	3.56–15	3.55–15	2.40–16	6.54–16	1.52–14	3.27–16	3.12–16	2.20–17	2.19–14	4.76–17	1.48–15
7.6	3.55–15	3.55–15	2.40–16	6.54–16	1.52–14	3.28–16	3.13–16	2.21–17	2.21–14	4.78–17	1.48–15
7.7	3.31–15	3.30–15	2.24–16	6.09–16	1.42–14	3.06–16	2.93–16	2.07–17	2.06–14	4.47–17	1.39–15
7.8	2.91–15	2.90–15	1.97–16	5.36–16	1.25–14	2.70–16	2.59–16	1.83–17	1.82–14	3.95–17	1.22–15
7.9	2.45–15	2.44–15	1.66–16	4.52–16	1.06–14	2.28–16	2.18–16	1.54–17	1.54–14	3.33–17	1.03–15
8.0	1.99–15	1.98–15	1.35–16	3.67–16	8.58–15	1.85–16	1.77–16	1.25–17	1.25–14	2.71–17	8.41–16
8.1	1.57–15	1.57–15	1.06–16	2.90–16	6.78–15	1.47–16	1.40–16	9.91–18	9.88–15	2.14–17	6.65–16
8.2	1.21–15	1.21–15	8.20–17	2.24–16	5.24–15	1.13–16	1.08–16	7.66–18	7.64–15	1.66–17	5.14–16
8.3	9.18–16	9.16–16	6.22–17	1.70–16	3.98–15	8.60–17	8.23–17	5.81–18	5.80–15	1.26–17	3.90–16
8.4	6.86–16	6.85–16	4.65–17	1.27–16	2.98–15	6.43–17	6.16–17	4.35–18	4.34–15	9.41–18	2.92–16
8.5	5.07–16	5.07–16	3.44–17	9.38–17	2.20–15	4.76–17	4.56–17	3.22–18	3.21–15	6.96–18	2.16–16
8.6	3.72–16	3.71–16	2.52–17	6.87–17	1.61–15	3.49–17	3.34–17	2.36–18	2.35–15	5.10–18	1.58–16
8.7	2.70–16	2.70–16	1.83–17	5.00–17	1.17–15	2.54–17	2.43–17	1.72–18	1.71–15	3.71–18	1.15–16
8.8	1.96–16	1.95–16	1.33–17	3.62–17	8.50–16	1.84–17	1.76–17	1.24–18	1.24–15	2.69–18	8.35–17
8.9	1.41–16	1.41–16	9.56–18	2.61–17	6.12–16	1.32–17	1.27–17	8.95–19	8.93–16	1.94–18	6.01–17
9.0	1.01–16	1.01–16	6.86–18	1.87–17	4.40–16	9.50–18	9.10–18	6.42–19	6.41–16	1.39–18	4.32–17
	s	e	k	l	d	c	j	a	b	m	n
6.0	2.07–35	7.22–35	2.12–34	1.75–35	9.24–36	2.02–36	2.99–34	5.86–35	2.03–36	2.11–35	9.98–37
6.1	9.46–31	3.35–30	1.02–29	8.49–31	4.50–31	9.81–32	1.47–29	2.98–30	1.03–31	1.13–30	5.32–32
6.2	4.43–27	1.59–26	5.02–26	4.16–27	2.21–27	4.83–28	7.32–26	1.52–26	5.26–28	5.96–27	2.81–28
6.3	3.39–24	1.23–23	3.99–23	3.31–24	1.77–24	3.85–25	5.89–23	1.25–23	4.31–25	5.03–24	2.38–25
6.4	6.18–22	2.25–21	7.48–21	6.21–22	3.32–22	7.24–23	1.11–20	2.40–21	8.30–23	9.91–22	4.68–23
6.5	3.59–20	1.32–19	4.46–19	3.69–20	1.98–20	4.32–21	6.69–19	1.46–19	5.04–21	6.13–20	2.90–21
6.6	8.44–19	3.12–18	1.07–17	8.84–19	4.75–19	1.04–19	1.61–17	3.54–18	1.22–19	1.51–18	7.14–20
6.7	9.65–18	3.58–17	1.24–16	1.03–17	5.51–18	1.20–18	1.87–16	4.16–17	1.44–18	1.80–17	8.49–19
6.8	6.23–17	2.31–16	8.07–16	6.69–17	3.60–17	7.85–18	1.23–15	2.74–16	9.48–18	1.20–16	5.65–18
6.9	2.55–16	9.50–16	3.33–15	2.76–16	1.49–16	3.25–17	5.09–15	1.14–15	3.95–17	5.02–16	2.37–17
7.0	7.28–16	2.72–15	9.59–15	7.95–16	4.28–16	9.34–17	1.47–14	3.30–15	1.14–16	1.46–15	6.90–17
7.1	1.56–15	5.83–15	2.07–14	1.71–15	9.24–16	2.01–16	3.17–14	7.16–15	2.48–16	3.18–15	1.50–16
7.2	2.66–15	9.96–15	3.54–14	2.94–15	1.58–15	3.46–16	5.44–14	1.23–14	4.26–16	5.49–15	2.59–16
7.3	3.79–15	1.42–14	5.06–14	4.20–15	2.26–15	4.94–16	7.78–14	1.77–14	6.11–16	7.89–15	3.73–16
7.4	4.67–15	1.75–14	6.26–14	5.19–15	2.80–15	6.11–16	9.63–14	2.19–14	7.57–16	9.81–15	4.63–16
7.5	5.14–15	1.93–14	6.90–14	5.72–15	3.09–15	6.74–16	1.06–13	2.42–14	8.37–16	1.09–14	5.13–16
7.6	5.16–15	1.94–14	6.95–14	5.76–15	3.11–15	6.79–16	1.07–13	2.44–14	8.44–16	1.10–14	5.18–16
7.7	4.83–15	1.81–14	6.51–14	5.40–15	2.91–15	6.35–16	1.00–13	2.29–14	7.91–16	1.03–14	4.86–16
7.8	4.26–15	1.60–14	5.75–14	4.77–15	2.58–15	5.62–16	8.87–14	2.02–14	7.00–16	9.11–15	4.30–16
7.9	3.60–15	1.35–14	4.86–14	4.03–15	2.18–15	4.74–16	7.49–14	1.71–14	5.91–16	7.71–15	3.64–16
8.0	2.93–15	1.10–14	3.96–14	3.28–15	1.77–15	3.87–16	6.10–14	1.39–14	4.82–16	6.28–15	2.97–16
8.1	2.31–15	8.70–15	3.13–14	2.60–15	1.40–15	3.06–16	4.83–14	1.10–14	3.82–16	4.98–15	2.35–16
8.2	1.79–15	6.73–15	2.42–14	2.01–15	1.08–15	2.37–16	3.74–14	8.54–15	2.95–16	3.85–15	1.82–16
8.3	1.36–15	5.11–15	1.84–14	1.53–15	8.23–16	1.80–16	2.84–14	6.49–15	2.24–16	2.93–15	1.38–16
8.4	1.02–15	3.82–15	1.38–14	1.14–15	6.17–16	1.34–16	2.13–14	4.86–15	1.68–16	2.19–15	1.04–16
8.5	7.52–16	2.83–15	1.02–14	8.44–16	4.56–16	9.95–17	1.57–14	3.59–15	1.24–16	1.62–15	7.67–17
8.6	5.51–16	2.07–15	7.47–15	6.19–16	3.35–16	7.30–17	1.15–14	2.64–15	9.12–17	1.19–15	5.63–17
8.7	4.01–16	1.51–15	5.44–15	4.51–16	2.44–16	5.31–17	8.40–15	1.92–15	6.64–17	8.67–16	4.10–17
8.8	2.91–16	1.09–15	3.94–15	3.26–16	1.76–16	3.85–17	6.08–15	1.39–15	4.81–17	6.28–16	2.97–17
8.9	2.09–16	7.87–16	2.84–15	2.35–16	1.27–16	2.77–17	4.38–15	1.00–15	3.46–17	4.52–16	2.14–17
9.0	1.50–16	5.65–16	2.04–15	1.69–16	9.12–17	1.99–17	3.14–15	7.19–16	2.49–17	3.25–16	1.53–17

Table 4. Recombination rate coefficients for DES lines of Ni XXVII forming Ni XXIVII (notation: *x–y* →*x* x10 $^{-y}$).

T(K)	α_R(cm^3 s^{-1})										
	o	p	v	u	r	q	i	h	t	s	g
6.0	8.63–39	9.75–39	5.48–40	1.20–39	1.90–38	4.00–40	9.66–40	1.49–41	1.71–38	3.84–40	1.13–41
6.1	1.90–33	2.15–33	1.25–34	2.79–34	4.80–33	1.05–34	2.58–34	3.97–36	4.64–33	1.06–34	3.12–36
6.2	3.10–29	3.50–29	2.08–30	4.75–30	8.77–29	1.97–30	4.90–30	7.55–32	8.96–29	2.06–30	6.08–32
6.3	6.40–26	7.24–26	4.40–27	1.01–26	1.98–25	4.54–27	1.14–26	1.76–28	2.12–25	4.91–27	1.45–28
6.4	2.57–23	2.90–23	1.79–24	4.17–24	8.52–23	1.99–24	5.04–24	7.77–26	9.43–23	2.20–24	6.49–26
6.5	2.79–21	3.15–21	1.97–22	4.63–22	9.80–21	2.32–22	5.92–22	9.12–24	1.11–20	2.62–22	7.73–24
6.6	1.08–19	1.22–19	7.70–21	1.82–20	3.96–19	9.47–21	2.43–20	3.74–22	4.60–19	1.09–20	3.20–22
6.7	1.83–18	2.07–18	1.32–19	3.13–19	6.96–18	1.68–19	4.33–19	6.67–21	8.24–18	1.95–19	5.75–21
6.8	1.61–17	1.83–17	1.17–18	2.79–18	6.32–17	1.54–18	3.97–18	6.12–20	7.59–17	1.80–18	5.31–20
6.9	8.48–17	9.59–17	6.18–18	1.48–17	3.40–16	8.30–18	2.15–17	3.31–19	4.12–16	9.80–18	2.89–19
7.0	2.95–16	3.34–16	2.16–17	5.17–17	1.20–15	2.95–17	7.66–17	1.18–18	1.47–15	3.51–17	1.03–18
7.1	7.40–16	8.36–16	5.43–17	1.30–16	3.06–15	7.53–17	1.96–16	3.02–18	3.77–15	8.99–17	2.65–18
7.2	1.43–15	1.62–15	1.05–16	2.53–16	5.98–15	1.48–16	3.85–16	5.92–18	7.42–15	1.77–16	5.22–18
7.3	2.25–15	2.54–15	1.66–16	3.99–16	9.49–15	2.35–16	6.12–16	9.43–18	1.18–14	2.82–16	8.32–18
7.4	3.00–15	3.39–15	2.22–16	5.34–16	1.27–14	3.16–16	8.25–16	1.27–17	1.59–14	3.81–16	1.12–17
7.5	3.52–15	3.97–15	2.60–16	6.27–16	1.50–14	3.73–16	9.73–16	1.50–17	1.88–14	4.50–16	1.33–17
7.6	3.71–15	4.20–15	2.75–16	6.63–16	1.59–14	3.96–16	1.03–15	1.59–17	2.00–14	4.79–16	1.41–17
7.7	3.61–15	4.08–15	2.67–16	6.46–16	1.56–14	3.87–16	1.01–15	1.56–17	1.96–14	4.68–16	1.38–17
7.8	3.29–15	3.72–15	2.44–16	5.89–16	1.42–14	3.54–16	9.24–16	1.42–17	1.79–14	4.29–16	1.26–17
7.9	2.85–15	3.22–15	2.11–16	5.10–16	1.23–14	3.07–16	8.02–16	1.24–17	1.55–14	3.72–16	1.10–17
8.0	2.36–15	2.67–15	1.75–16	4.24–16	1.02–14	2.55–16	6.68–16	1.03–17	1.29–14	3.10–16	9.14–18
8.1	1.90–15	2.15–15	1.41–16	3.41–16	8.24–15	2.05–16	5.37–16	8.28–18	1.04–14	2.49–16	7.36–18
8.2	1.49–15	1.68–15	1.10–16	2.67–16	6.46–15	1.61–16	4.21–16	6.49–18	8.16–15	1.96–16	5.77–18
8.3	1.14–15	1.29–15	8.46–17	2.05–16	4.96–15	1.24–16	3.23–16	4.98–18	6.27–15	1.50–16	4.43–18
8.4	8.59–16	9.72–16	6.38–17	1.54–16	3.74–15	9.33–17	2.44–16	3.76–18	4.73–15	1.13–16	3.34–18
8.5	6.40–16	7.23–16	4.75–17	1.15–16	2.79–15	6.95–17	1.82–16	2.80–18	3.53–15	8.45–17	2.49–18
8.6	4.71–16	5.33–16	3.50–17	8.47–17	2.05–15	5.12–17	1.34–16	2.07–18	2.60–15	6.23–17	1.84–18
8.7	3.44–16	3.89–16	2.56–17	6.19–17	1.50–15	3.75–17	9.80–17	1.51–18	1.90–15	4.56–17	1.34–18
8.8	2.50–16	2.83–16	1.86–17	4.50–17	1.09–15	2.72–17	7.12–17	1.10–18	1.38–15	3.31–17	9.76–19
8.9	1.81–16	2.04–16	1.34–17	3.25–17	7.88–16	1.97–17	5.15–17	7.93–19	9.98–16	2.39–17	7.05–19
9.0	1.30–16	1.47–16	9.65–18	2.34–17	5.67–16	1.41–17	3.70–17	5.70–19	7.18–16	1.72–17	5.07–19
	f	e	k	l	d	c	j	a	b	m	n
6.0	7.63–41	1.45–38	1.41–38	1.34–38	2.48–39	2.46–39	4.76–38	9.70–39	3.80–40	2.98–39	8.51–40
6.1	2.10–35	4.09–33	4.12–33	3.94–33	7.33–34	7.26–34	1.44–32	3.04–33	1.19–34	9.81–34	2.79–34
6.2	4.09–31	8.12–29	8.46–29	8.09–29	1.51–29	1.50–29	3.03–28	6.56–29	2.57–30	2.20–29	6.28–30
6.3	9.75–28	1.96–25	2.10–25	2.01–25	3.76–26	3.73–26	7.67–25	1.69–25	6.64–27	5.87–26	1.67–26
6.4	4.37–25	8.89–23	9.71–23	9.29–23	1.75–23	1.73–23	3.60–22	8.10–23	3.17–24	2.87–23	8.19–24
6.5	5.20–23	1.07–20	1.18–20	1.13–20	2.14–21	2.12–21	4.45–20	1.01–20	3.97–22	3.67–21	1.05–21
6.6	2.16–21	4.45–19	5.01–19	4.79–19	9.07–20	8.98–20	1.90–18	4.38–19	1.72–20	1.61–19	4.58–20
6.7	3.87–20	8.04–18	9.15–18	8.74–18	1.66–18	1.64–18	3.50–17	8.12–18	3.18–19	3.02–18	8.60–19
6.8	3.57–19	7.46–17	8.55–17	8.18–17	1.55–17	1.54–17	3.29–16	7.69–17	3.01–18	2.89–17	8.23–18
6.9	1.94–18	4.07–16	4.70–16	4.50–16	8.54–17	8.46–17	1.82–15	4.27–16	1.67–17	1.62–16	4.61–17
7.0	6.96–18	1.46–15	1.70–15	1.62–15	3.08–16	3.06–16	6.58–15	1.55–15	6.09–17	5.92–16	1.69–16
7.1	1.78–17	3.76–15	4.38–15	4.19–15	7.96–16	7.89–16	1.70–14	4.04–15	1.58–16	1.54–15	4.40–16
7.2	3.51–17	7.41–15	8.66–15	8.28–15	1.58–15	1.56–15	3.38–14	8.02–15	3.14–16	3.08–15	8.78–16
7.3	5.60–17	1.18–14	1.39–14	1.33–14	2.52–15	2.50–15	5.42–14	1.29–14	5.06–16	4.97–15	1.42–15
7.4	7.56–17	1.60–14	1.88–14	1.79–14	3.42–15	3.39–15	7.35–14	1.75–14	6.87–16	6.77–15	1.93–15
7.5	8.93–17	1.89–14	2.22–14	2.13–14	4.05–15	4.01–15	8.72–14	2.08–14	8.16–16	8.05–15	2.30–15
7.6	9.50–17	2.01–14	2.37–14	2.27–14	4.32–15	4.28–15	9.30–14	2.22–14	8.71–16	8.61–15	2.46–15
7.7	9.30–17	1.97–14	2.32–14	2.22–14	4.23–15	4.19–15	9.12–14	2.18–14	8.54–16	8.46–15	2.41–15
7.8	8.51–17	1.80–14	2.13–14	2.03–14	3.88–15	3.84–15	8.36–14	2.00–14	7.84–16	7.77–15	2.22–15
7.9	7.39–17	1.57–14	1.85–14	1.77–14	3.37–15	3.34–15	7.27–14	1.74–14	6.82–16	6.77–15	1.93–15
8.0	6.15–17	1.30–14	1.54–14	1.47–14	2.81–15	2.78–15	6.06–14	1.45–14	5.69–16	5.65–15	1.61–15
8.1	4.95–17	1.05–14	1.24–14	1.19–14	2.26–15	2.24–15	4.88–14	1.17–14	4.58–16	4.55–15	1.30–15
8.2	3.88–17	8.24–15	9.74–15	9.31–15	1.78–15	1.76–15	3.83–14	9.19–15	3.60–16	3.58–15	1.02–15
8.3	2.98–17	6.32–15	7.48–15	7.15–15	1.36–15	1.35–15	2.95–14	7.06–15	2.77–16	2.75–15	7.83–16
8.4	2.25–17	4.78–15	5.65–15	5.40–15	1.03–15	1.02–15	2.23–14	5.33–15	2.09–16	2.08–15	5.92–16
8.5	1.68–17	3.56–15	4.21–15	4.03–15	7.68–16	7.61–16	1.66–14	3.98–15	1.56–16	1.55–15	4.42–16
8.6	1.24–17	2.62–15	3.11–15	2.97–15	5.67–16	5.61–16	1.22–14	2.93–15	1.15–16	1.14–15	3.26–16
8.7	9.04–18	1.92–15	2.27–15	2.17–15	4.14–16	4.10–16	8.95–15	2.15–15	8.41–17	8.36–16	2.38–16
8.8	6.57–18	1.39–15	1.65–15	1.58–15	3.01–16	2.98–16	6.50–15	1.56–15	6.11–17	6.08–16	1.73–16
8.9	4.75–18	1.01–15	1.19–15	1.14–15	2.17–16	2.15–16	4.70–15	1.13–15	4.42–17	4.39–16	1.25–16
9.0	3.41–18	7.25–16	8.58–16	8.20–16	1.56–16	1.55–16	3.38–15	8.11–16	3.18–17	3.16–16	9.01–17

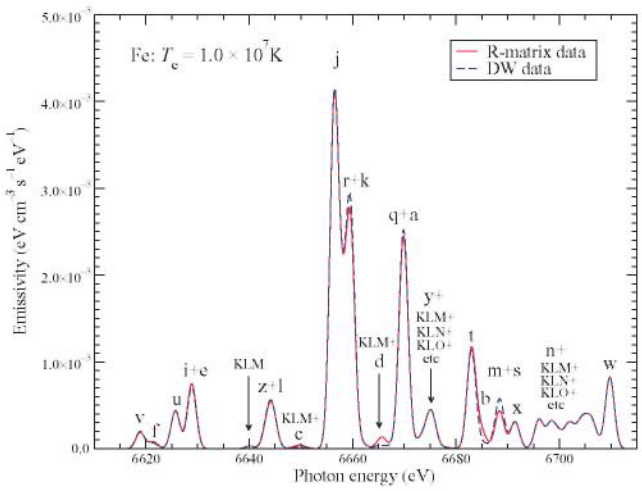

Figure 4. Comparison of theoretical DES spectra of He-like Fe XXV at $T = 10^7$ K using the present DES strengths using the unified recombination method (solid, red line) and the distorted wave (DW) data from the Los Alamos codes (blue, dashed line).

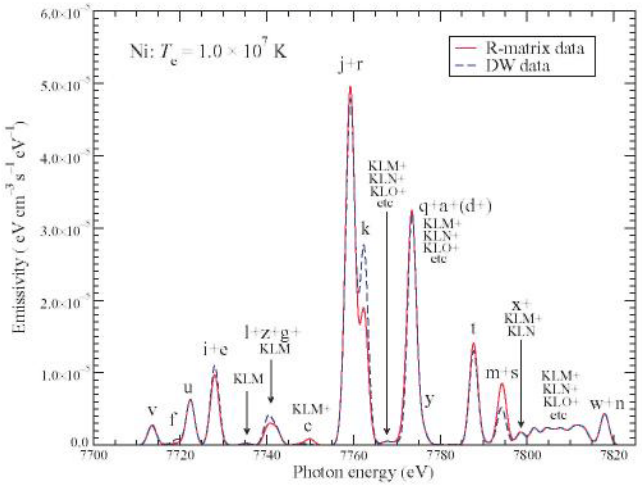

Figure 5. Comparison of theoretical DES spectra of He-like Ni XXVII at $T = 10^7$ K, as in figure 4.

AI rates computed from Los Alamos National Laboratory (LANL) suite of atomic physics codes (see: Abdallah *et al* 1994, 2001). We get very good agreement between the DES spectra computed using the two sets of data, as shown in figures 4 and 5. The calculations for both ions generally follow the approach outlined in Oelgoetz *et al* (2007a) for the RM data set, as to data sources and the complete statistical models. The major exception to this is that both models presented use level energies calculated by the LANL code CATS (see Abdallah *et al* 1994, 2001) for all energy levels except those that give rise to the KLL satellite lines. The energies for these autoionizing states are taken from the data presented in this work. Both models use identical energies to facilitate an easy comparison of their spectra. The two models differ from each other in that the R-matrix curve presented here uses AI rates calculated from the KLL DES strengths as computed herein, and the DW data set uses distorted wave AI rates calculated using the LANL code GIPPER (again, see Abdallah *et al* 1994, 2001).

5. Conclusion

The main conclusions of this work are:

- The theoretical and computational framework for self-consistent and unified treatment of photoionization and radiative and dielectronic recombination has now extended the calculation of DES strengths. Computed DES spectra demonstrate the effect of channel interference and overlapping profiles, though the practical effect on rate coefficients is small.
- Theoretical formulation for AI rates from the unified satellite line strengths is given for applications in astrophysical models based on IRA methodologies. The first comparison for Fe XXV and Ni XXVII spectra shows excellent agreement with data from the Los Alamos National Laboratory suite of atomic physics codes.
- Recombination rate coefficients are presented for all 22 KLL DES lines of Fe XXV and Ni XXVII for a wide temperature range. We find considerable differences with earlier works of more than 20% at low temperatures $<10^7$ K, but the agreement improves to <10% towards the temperature of maximum abundance for both ions. While we expect the present rate coefficients to be more accurate, a conservative estimate of uncertainties in the temperature range of practical applications, $T > 10^7$ K, is about 10–20%.
- Intensity ratios $I(s)/I(w)$ of the DES to w-line of He-like Fe and Ni are theoretically computed for practical applications in high-temperature x-ray plasmas.
- Although the present unified dielectronic resonance strengths are in good agreement with those computed in previous works using the IRA, some significant differences are found in temperature ranges where the DES are most temperature sensitive, below the temperature of maximum abundance of He-like ions in coronal equilibrium.

Acknowledgments

This work was supported partially by the NASA Astrophysical Theory Program and the Space Astrophysical Research and Analysis programs as well partially conducted under the auspices of the United States Department of Energy at Los Alamos National Laboratory. Much of the computational work was carried out at the Ohio Supercomputer Center in Columbus, Ohio.

References

Abdallah J, Clark R E H, Peek J M and Fontes C J 1994 *J. Quant. Spectrosc. Radiat. Transfer* **51** 1

Abdallah J, Zhang H L, Fontes C J, Kilcrease D P and Archer B J 2001 *J. Quant. Spectrosc. Radiat. Transfer* **71** 107

Beiersdorfer P, Philips T W, Wong K L, Marrs R E and Vogel D A 1992 *Phys. Rev.* A **46** 3812

Berrington K A, Burke P G, Butler K, Seaton M J, Storey P J, Taylor K T and Yan Y 1987 *J. Phys.* B **20** 6379

Berrington K A, Eissner W and Norrington P H 1995 *Comput. Phys. Commun.* **92** 290

Bely-Dubau F, Dubau J, Faucher P and Gabriel A H 1982 *Mon. Not. R. Astron. Soc.* **198** 239

Eissner W, Jones M and Nussbaumer H 1974 *Comput. Phys. Commun.* **8** 270

Gabriel A H 1972 *Mon. Not. R. Astron. Soc.* **160** 99

Hummer D G, Berrington K A, Eissner W, Pradhan A K, Saraph H E and Tully J A 1993 *Astron. Astrophys.* **279** 298
Kato T, Fujiwara T and Hanaoka Y 1998 *Astrophys. J.* **492** 822
Nahar S N 2005 *Astrophys. J. Suppl. Ser.* **158** 80
Nahar S N and Pradhan A K 1994 *Phys. Rev.* A **49** 1816
Nahar S N and Pradhan A K 2004 Review in *Radiation Processes in Physics and Chemistry* **70** 323
Nahar S N and Pradhan A K 2006 *Phys. Rev.* A **73** 062718-1
Nahar S N, Pradhan A K and Zhang H L 2000 *Astrophys. J. Suppl. Ser.* **131** 375
Nahar S N, Pradhan A K and Zhang H L 2001 *Astrophys. J. Suppl. Ser.* **133** 255
Oelgoetz J 2006 *PhD Thesis* The Ohio State University Oelgoetz J, Fontes C J, Zhang H L, Montenegro M, Nahar S N and Pradhan A K 2007a *Mon. Not. R. Astron. Soc.* **382** 761
Oelgoetz J, Fontes C J, Zhang H L and Pradhan A K 2007b *Phys. Rev.* A **76** 062504-1
Oelgoetz J and Pradhan A K 2001 *Mon. Not. R. Astron. Soc.* **327** L42
Oelgoetz J and Pradhan A K 2004 *Mon. Not. R. Astron. Soc.* **354** 1093
Pradhan A K 1985 *Astrophys. J. Suppl. Ser.* **59** 183
Pradhan A K and Zhang H L 1997 *J. Phys.* B **30** L571
Sakimoto K, Terao M and Berrington K A 1990 *Phys. Rev.* A **42** 291
Vainshtein L A and Safronova U I 1978 *At. Data Nucl. Data Tables* **25** 49
Whiteford A D, Badnell N R, Ballance C P, O'Mullane M G, Summers H P and Thomas A L 2001 *J. Phys.* B **34** 3179
Zhang H L, Nahar S N and Pradhan A K 1999 *J. Phys.* B **32** 1459